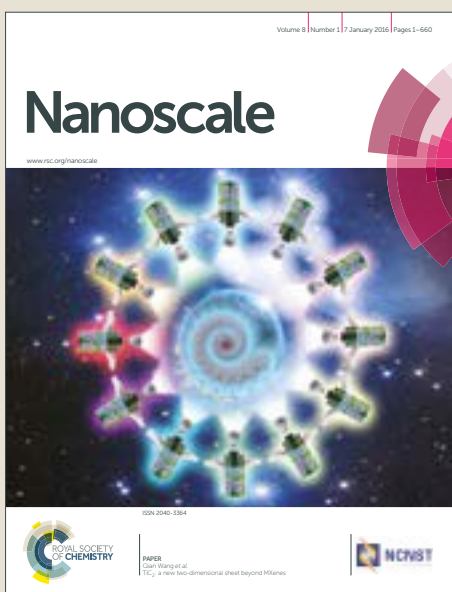


Nanoscale

Accepted Manuscript



This article can be cited before page numbers have been issued, to do this please use: K. Z. Milowska, M. Ghorbani-Asl, M. Burda, L. Wolanicka, N. Catic, P. Bristowe and K. Koziol, *Nanoscale*, 2017, DOI: 10.1039/C7NR02142A.



This is an Accepted Manuscript, which has been through the Royal Society of Chemistry peer review process and has been accepted for publication.

Accepted Manuscripts are published online shortly after acceptance, before technical editing, formatting and proof reading. Using this free service, authors can make their results available to the community, in citable form, before we publish the edited article. We will replace this Accepted Manuscript with the edited and formatted Advance Article as soon as it is available.

You can find more information about Accepted Manuscripts in the [author guidelines](#).

Please note that technical editing may introduce minor changes to the text and/or graphics, which may alter content. The journal's standard [Terms & Conditions](#) and the ethical guidelines, outlined in our [author and reviewer resource centre](#), still apply. In no event shall the Royal Society of Chemistry be held responsible for any errors or omissions in this Accepted Manuscript or any consequences arising from the use of any information it contains.

Journal Name

ARTICLE TYPE

Cite this: DOI: 10.1039/xxxxxxxxxx

Breaking the Electrical Barrier between Copper and Carbon Nanotubes[†]

Karolina Z. Milowska,^{*a} Mahdi Ghorbani-Asl,^{*ab} Marek Burda,^a Lidia Wolanicka,^a Nordin Ćatić,^a Paul D. Bristowe^a and Krzysztof K. Koziol^{*a‡}

Received Date

Accepted Date

DOI: 10.1039/xxxxxxxxxx

www.rsc.org/journalname

Improving the interface between copper and carbon nanotubes (CNTs) offers a straightforward strategy for the effective manufacturing and utilisation of Cu-CNT composite material that could be used in various industries including microelectronics, aerospace and transportation. Motivated by a combination of structural and electrical measurements on Cu-M-CNT bimetal systems (M = Ni, Cr) we show, using first principles calculations, that the conductance of this composite can exceed that of a pure Cu-CNT system and that the current density can even reach 10^{11} A/cm². The results show that the proper choice of alloying element (M) and type of contact facilitate the fabrication of ultra-conductive Cu-M-CNT systems by creating a favourable interface geometry, increasing the interface electronic density of states and reducing the contact resistance. In particular, a small concentration of Ni between the Cu matrix and the CNT using either an "end contact" and or a "dot contact" can significantly improve the electrical performance of the composite. Furthermore the predicted conductance of Ni-doped Cu-CNT "carpets" exceeds that of an undoped system by ~200%. Cr is shown to improve CNT integration and composite conductance over a wide temperature range while Al, at low voltages, can enhance the conductance beyond that of Cr.

1 Introduction

The progressive miniaturisation of electronic devices¹ and increasing demand for electrical power due to the growing human population in a changing environment² requires utilisation of new materials for electrical wires and interconnects. Since conventional conductors are mostly based on copper and copper alloys, any new material needs to be compatible with large-scale conductor manufacturing. The combination of Cu and carbon nanotubes (CNTs) holds great promise for the fabrication of novel conductors with superior electrical and thermal performance when compared to conventional conductors³. Copper offers high concentrations of free electrons while CNTs not only provide a high mobility conductance channel to transport these free electrons with weaker scattering than copper⁴, but also mechanically reinforces the composite, improves its flexibility, and reduces weight^{5–7}. In

particular, the specific electrical conductivity of a Cu-CNT composite compared to Cu has been enhanced by 40%, ampacity 100 times⁸, yield strength 2.3 times⁹ and ultimate tensile strength almost 3 times¹⁰. The thermal expansion coefficient has been reported to be comparable with that of silicon¹¹. This makes Cu-CNT composites unrivalled candidates for an extremely wide range of applications starting from microscale electronics, inverters and battery interconnects in commonly-used devices to macroscale applications in the transportation industry which typically require lightweight conductors.

However, uniform integration of CNTs into the metal matrix is still a significant challenge¹². Issues of non-uniform CNT dispersion leading to the formation of clusters in the Cu matrix and a weak Cu-C interphase boundary, which are common problems for most processing techniques, can lead to complete separation of the incompatible phases as shown in Fig. 1 (a). Better incorporation of the CNTs into the Cu matrix is a prerequisite for complete utilisation of the superior properties of the composites. This can be achieved through direct functionalization of the CNTs or modification of the copper matrix. Covalent functionalization of the CNTs enables improved bonding with the composite matrix and their debundling¹³, but it may lead to certain unwanted changes in the CNT's mechanical and electronic properties¹⁴. Adsorbates form covalent bonds to the lateral surface of the CNTs, causing local deformations, sp² to sp³ rehybridization,

^a Department of Materials Science and Metallurgy, University of Cambridge, 27 Charles Babbage Rd, CB3 0FS Cambridge, United Kingdom. E-mail: karolina.milowska@gmail.com

^b Institute of Ion Beam Physics and Materials Research, Helmholtz-Zentrum Dresden-Rossendorf, 01314 Dresden, Germany. E-mail: mahdi.ghorbani@hzdr.de

† Electronic Supplementary Information (ESI) available. See DOI: 10.1039/b000000x/

‡ Present address: Cranfield University, School of Aerospace, Transport and Manufacturing, Building 61, Cranfield, Bedfordshire, MK43 0AL, United Kingdom. Tel: +44 (0) 1234 754038; E-mail: k.koziol@cranfield.ac.uk

possible formation of heptagon/pentagon defects, vacancies, and substitutional doping depending on the type and concentration of the particular functionals, and as a consequence hamper the conducting sub-bands^{14–16}. Non-covalent functionalization, mainly based on supramolecular complexation using various adsorption forces, maintains CNT structure^{17,18} but its feasibility in multi-walled CNTs is limited to the outer wall, while inner walls remain electrically inactive. On the other hand, addition of one or several active components to the nonreactive copper matrix may constitute an effective and economic way of improving the wettability in the Cu-CNT system (Fig. 1 (b)), on condition that the doping metal (alloying element) is highly active in the copper matrix^{12,19,20} (Fig. S1). Consequently, utilisation of the properties of CNTs in copper matrix composites calls for a treatment that improves electron and heat transfer between the reinforcement and the matrix. This requires a full understanding of the interface between the constituents in order to create an efficient mechanical and electrical connection between them.

On the theoretical side, previous computational studies have been directed towards the electronic and transport characteristics of single-walled CNTs connected to various metals for nanoelectronic applications²¹ mainly focusing on "end"^{22–24} or "side"^{21,25–28} type contacts. The model employed in those studies assumed the presence of a metal matrix as an electrode, while most of the nanotube backbone was free standing in a vacuum. However, a Cu-CNT or Cu-M-CNT composite model requires full embedding of the CNT into the metal matrix to account for structural and electronic changes induced by their interaction. This is beyond a simple continuum model^{4,29} or a classical molecular dynamics approach^{30,31}, and can only be effectively studied using large-scale ab-initio calculations³². Previous discussions^{4–9} have already indicated that such an investigation, even though being extremely computationally demanding, is essential for a full understanding of the physical mechanisms governing the extraordinary performance of metal-CNT composites.

In the present paper, we demonstrate an effective and practical way of enhancing the electrical transport properties of a Cu-CNT system. We begin by presenting experimental evidence for the advantages of alloying the Cu matrix with Cr or Ni to improve the wettability and conductance of such a system containing multi-walled nanotubes. The results indicate that alloying is beneficial and motivated by this we then present some first principles calculations on various model Cu-M-CNT systems to gain physical insight into the microscopic origins of the effects observed. Computationally we have investigated the influence of three alloying elements, Ni, Cr and Al, on the structural stability and transport properties a Cu-CNT system in which the contact is of the side, end, fully embedded and dot type. The main CNT studied is (5,5) but calculations on a (10,10), (6,4), and a double-walled CNT (10,10)@(5,5) are also presented. We have also considered a "carpet" configuration, which is a dense arrangement of vertically aligned CNTs as shown in Fig. 5 (f). We find that a small concentration of Ni located between the Cu matrix and the CNT can significantly improve the electrical performance of the composite. In particular, the predicted conductance of Ni-doped Cu CNT carpets exceeds that of an undoped system by a factor of two. Cr

greatly improves CNT integration in the Cu matrix and can also rival the conductance of the undoped composite in the temperature range 20 - 377° C, especially if the oxidation during the fabrication process is eliminated. For small applied biases, Al can improve the electrical properties of the composite even more than Cr. The calculations indicate that three main factors are responsible for the enhanced current injection at a metal-CNT contact: (i) favourable interface geometry and bonding, (ii) high density of interface electronic states which can contribute to the transmission, and (iii) reduced contact resistance between the CNTs and the Cu matrix.

2 Results and discussion

2.1 Experiments

Cr and Ni were chosen for incorporation into the Cu matrix due to their strong interaction with carbon and copper. Ni, among other non-reactive metals with high carbon solubility, is commonly used to alloy the Cu matrix. It has a rather small influence on the thermal and electrical conductance of Cu but enhances the mechanical properties^{19,20,33,34}. On the other hand, Cr is a representative of carbide forming metals and, contrary to Ti, does not destroy the CNT structure and becomes less easily oxidized^{33,34}. Cu-M-CNT composites were prepared by depositing vertically aligned multi-walled carbon nanotubes (MWCNT) onto a substrate (see Fig. 1 (c)) and then coating the layer with Cu, Cu/Ni or Cu/Cr using magnetron sputtering followed by an annealing heat treatment. The performance of all three types of samples was analysed in different annealing temperatures by scanning electron microscopy (SEM), energy-dispersive X-ray (EDX) mapping and Raman Spectroscopy.

First we present results for the pure Cu-CNT system, i.e. vacuum heat-treated copper sputtered onto MWCNTs. Because of melting-point depression³⁵ the nanoscale sputtered copper coating appears to melt at temperatures as low as 400° C and subsequently forms spherical submicron-sized particles that do not wet the CNTs. Intense melt vaporization at a temperature of about 1000° C leads to complete removal of the copper coating as depicted in Fig. 2 (a) and Fig.S3 (a) in the ESI†. This causes the formation of large voids around the CNTs in the Cu matrix as shown in Fig. 1 (a).

As opposed to pure copper, Ni dissolves relatively large amounts of carbon. SEM analysis of the Cu-Ni-CNT system, presented in Fig. 3 (a), reveals signs of defects on the surface of the MWCNTs that were heated up to 600° C. Raman Spectroscopy results, shown in Fig.S4 (b) in the ESI†, corroborate these observations showing an increase in the intensity ratio (I_D/I_G) of the defect-induced band (D) to the graphitic vibration band (G) with increasing target temperature of the vacuum heat treatment. Moreover, combined SEM and EDX characterization of the Cu-Ni-CNT system (Fig.S2 (a) and Fig.S3 (b) in the ESI†) shows a formation of a CuNi solid solution with significant carbon solubility and diffusivity. Dissolution of carbon in Ni leads to the formation of a macroscopically concave solid/liquid interface³⁶. The solubility of carbon in nickel (max. 0.18 wt%) is reduced as the copper content increases (0.01 wt% for 90 wt% Cu concentration) while

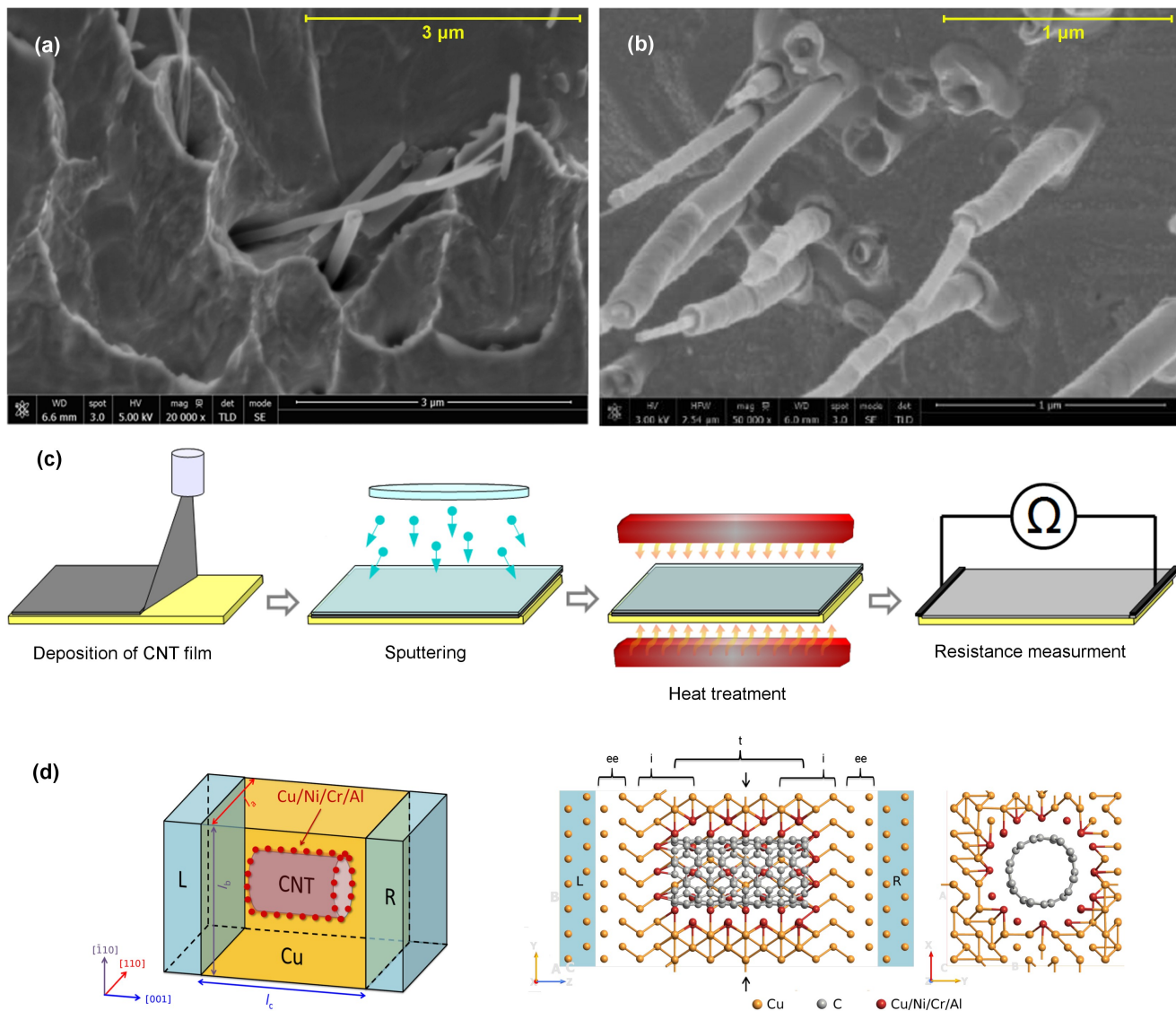


Fig. 1 Cu-CNT and Cu-M-CNT composites, fabrication and computational model. (a) SEM image of the Cu-CNT composite showing the formation of large voids around the CNTs. (b) SEM image of the Cu-Cr-CNT composite depicting the infiltration of Cu-Cr alloys into the voids with simultaneous formation of a new compound at the phase boundary. Lower side of a Cu 1.2 wt.% Cr sessile drop formed during vacuum heating up to 1200° C (c) Experimental setup for studying interactions between the CNTs and metal matrix. (d) The schematic view of the model used for the transport calculations of Cu-M-CNT (M = Cu, Ni, Cr, and Al) systems. The central part (yellow) was used for structural properties analysis. The semi-infinite electrodes consisting of perfect copper are depicted in blue. The atomistic side and cross-sectional views of the model are presented next to the 3D visualization. Black arrows on the side view indicate the position of the cross-section. For clarity, some metal layers were removed. ee stands for the extended electrode region, i is the interface region and t is the transport region.

Cu and Ni are mutually soluble in any amount (unlimited solid solubility) both in the liquid and solid phase. Consequently, such alloying can significantly increase the conductance of the composite due to the formation of direct contacts to a large number of inner CNT walls. However, the results also show a destructive influence of Ni on the CNT structure. Therefore, controlling the reactions appears to be much more complicated than in the case of conventional macroscopic carbon materials allowing the formation of a several micron thick interface layer.

As an alternative to Ni, we have tested the possibility of using Cr to alloy the Cu matrix and enhance interaction with the CNTs.

Pure chromium reacts with carbon to form carbides that are characterised by relatively good electrical and thermal conductivities³⁷. Good adhesion and wetting observed between Cu and chromium carbides³⁸ can be explained by the formation of metallic bonding at the interface, although covalent and other types of interactions (e.g. dispersion) cannot be excluded³⁹. Similar to the Cu-CNT system, the sputtered Cr coating melts at lower temperatures than expected at the macroscale. SEM analysis of the Cu-Cr-CNT system, presented in Fig. 3 (b), reveals the formation of Cr or a Cr carbide phase at the interface between the CNT and the Cu matrix. Lack of an unequivocal copper wetting tran-

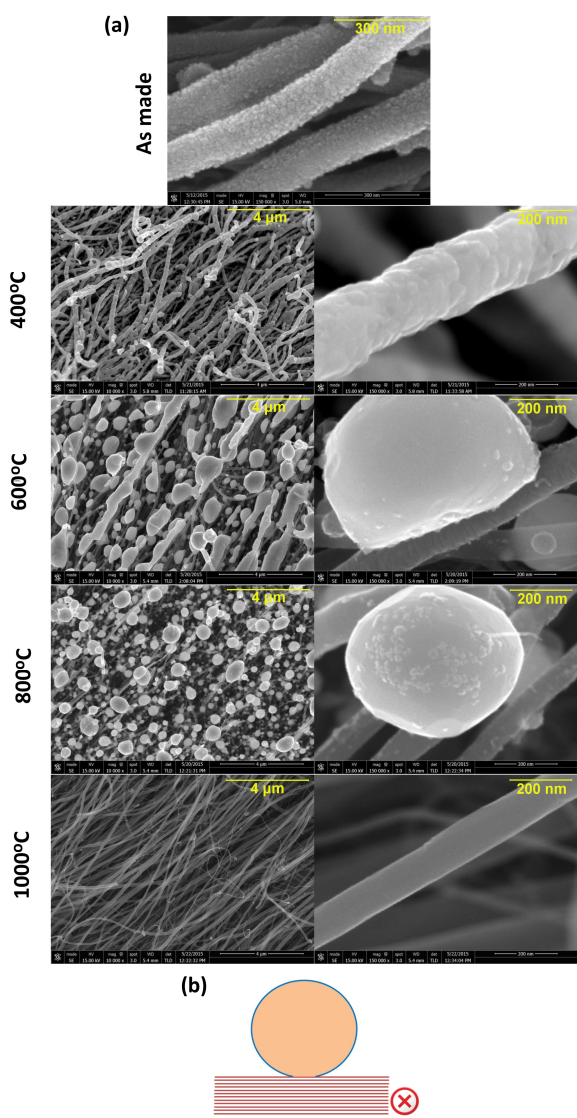


Fig. 2 Structure of the Cu-CNT system. (a) SEM images of Cu sputtered onto vertically aligned MWCNTs before and after vacuum heat-treatment at 400° C, 600° C, 800° C and 1000° C. (b) Schematic representation of contact formation between CNT walls and the metal matrix. The red cross indicates that there is no useful contact.

sition (non-wetting to a wetting system) can be explained by the formation of a non-continuous layer of wettable Cr-phase, which hinders the copper spreading over the substrate (see Fig.S2 (b) in the ESI†). EDX data are given in Fig.S3 (c) in the ESI†. Based on the SEM analysis it can be concluded that heat-treating the Cu-Cr-CNT system may lead to conduction through the outer CNT walls only. This effect can be attributed to the negligibly small solubility of carbon in chromium and the formation of Cr carbides. The process occurs at the cost of a few outer walls of the MWCNTs, as schematically illustrated in Fig. 3 (d). Our experiments show (see Fig.S1 in the ESI†) that the optimal concentration of alloying element in the composite is between 0.05 and 0.13 wt.%. Cr. The CNT fibre was not pushed out of the molten sample by surface tension, which indicates the fibre was wetted by the me-

tal. In this case the reaction layer was minimal, as there was no significant damage to the CNT.

To test predictions that alloying the Cu matrix could improve the electrical performance of a Cu-CNT composite we have performed macroscale resistance measurements. Multi-walled CNT tracks were deposited onto quartz plates and then metal sputtered and vacuum heat-treated as shown schematically in Fig. 1 (c). This procedure effectively removed contamination and densified the CNT network. The conductance of non-sputtered CNT tracks is found to increase by about 35% after annealing, whereas for Cu, Cr and Ni sputtered tracks the increase on average is about 44%, 47%, and 123% respectively (see Tab.S1 in the ESI†). The measured conductance values are shown in Fig. 5 (c) inset. Ni produces the greatest reduction in contact resistance between individual carbon nanotubes. It is important to note that the increase in conductance of the sputtered tracks is not due to the presence of the metal coatings on their own. By themselves the sputtered pure metals have very low conductance, for example for Ni and Cr it is on the order of 10^{-4} S and 10^{-5} S respectively. Although the electrical measurements have not been made on alloyed systems, they clearly show that Ni can significantly increase the conductance of the MWCNTs and, according to the deposition experiments, this is due to the formation of contacts to a large number of inner walls and hence their participation in the conduction.

In summary, the experiments described above indicate that (i) appropriate alloying of the Cu matrix of a Cu-CNT composite can improve its wettability and hence degree of contact between the metal and CNT, and (ii) of the alloying metals tested Ni increases the conductance of the composite system the most. The results clearly suggest that partial doping of the Cu matrix could be an effective way of enhancing interaction between multi-wall carbon nanotubes and Cu on the macroscale, thus improving the overall conductance of a Cu-CNT composite. To understand these interactions better and also the transport processes involved, we now present some first principles calculations on various model Cu-M-CNT systems. These systems are, by necessity, much simpler than those experimentally observed, but nevertheless provide useful fundamental understanding at the atomic level.

2.2 Calculations

To explore the structural and electronic properties of model Cu-M-CNT bimetallic composites, we have constructed a computational block of optimised fcc Cu, oriented as depicted in Fig. 1 (d), into which we cut a cylinder of predefined size for a particular CNT. Periodic boundary conditions are applied to the central region. The size of the cavity and orientation of the CNT inside was carefully chosen to minimise the lattice mismatch between the metal and the CNT^{26,32} including optimal separation distance between the Cu and C atoms ($1.9\text{--}2.4$ Å^{22,23}). Alloying elements M were introduced as a full or partial replacement of the first Cu layer around the CNT creating "embedded", "end", "dot", and "side" contact types as illustrated in Fig. 4. For the end contact, only those Cu atoms that are immediately adjacent to both ends of the nanotube are replaced with M atoms. The side contact incorporates

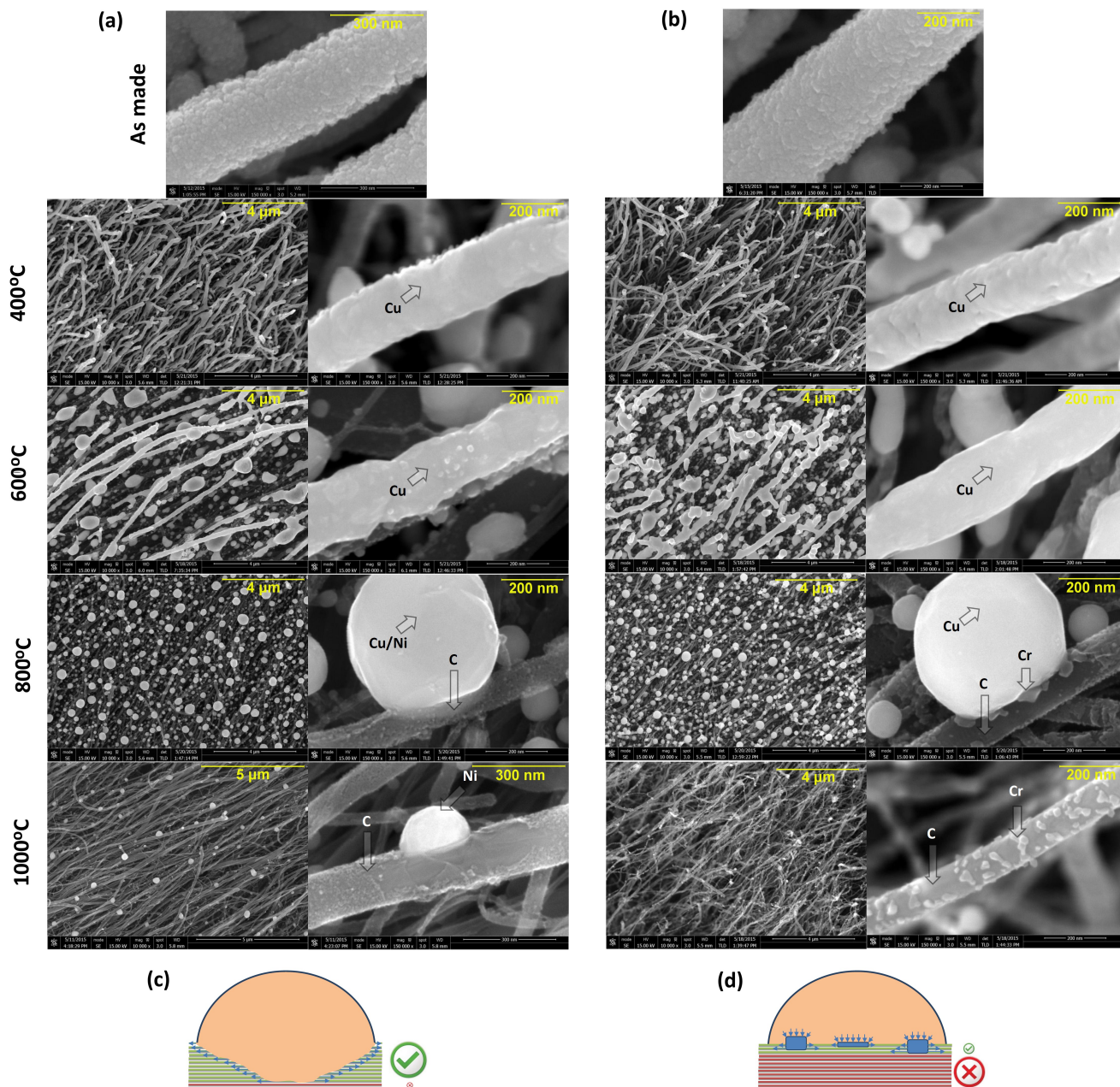


Fig. 3 Structure of the Cu-M-CNT systems. SEM images of (a) Cu/Ni and (b) Cu/Cr sputtered onto vertically aligned MWCNTs before and after vacuum heat-treatment at 400° C, 600° C, 800° C and 1000° C (c), (d) Schematic representations of contact formation between CNT walls and the metal matrix. The green tick indicates that contact is made with most walls but the red cross indicates that contact is only made with a few walls highlighted in blue.

a layer of M atoms around the lateral surface of the CNT while the embedded contact is a simple combination of end and side contact that completely covers the CNT. Finally, the dot contact, which is the smallest in size, takes the shape of a truncated cone containing only four replaced Cu atoms above the lateral surface of the CNT and two additional M atoms introduced in between the Cu matrix and the CNT. For the alloying elements, we have chosen three metals with interesting properties: Ni, Cr and Al. Ni interacts strongly with C²⁸ and is soluble in Cu⁴⁰. Cr is an n-type dopant in CNTs²¹ but decreases the conductivity of Cu⁴⁰. Al

weakly physisorbs on CNT surfaces as nanoparticles⁴¹ and also decreases the conductivity of Cu⁴⁰ but has the potential to create almost three times more conductive contacts to CNTs than Cu²⁴. Most of the structural and electronic property calculations were performed using a rectangular 7x7x16 atom supercell with dimensions $l_a=l_b=18.2 \text{ \AA}$ and $l_c=30 \text{ \AA}$ into which a (5,5) nanotube is inserted about 14 Å long (see Fig. 1 (d)). However, we have also considered a CNT with a larger diameter - (10,10), a CNT which is chiral - (6,4), and a CNT which has a double wall - (10,10)@(5,5). The largest supercell considered (the double

Table 1 Structural and electronic properties of all studied types of Cu-M-CNT composites (M=Cu, Ni, Cr, Al): coefficients of variation of nanotube radius (CV), interfacial strengths τ , matrix surface energies γ , and electrostatic potential barriers between metal matrix and nanotube ($\Delta\bar{V}_H$).

system	contact	CV	τ (J/m ²)	γ (J/m ²)	$\Delta\bar{V}_H^{left}$ (eV)	$\Delta\bar{V}_H^{right}$ (eV)
Cu-(5,5)	embedded	0.044	2.66	2.74	1.503	1.551
Cu-Ni-(5,5)	end	0.043	3.72	3.26	1.162	1.070
	dot	0.085	3.01	3.04	1.516	1.513
	side	0.065	4.26	4.12	1.559	1.704
	embedded	0.090	3.11	4.25	1.229	1.207
Cu-Cr-(5,5)	end	0.057	2.79	2.56	1.380	1.362
	side	0.064	3.05	2.45	1.601	1.534
	embedded	0.075	3.29	3.24	1.366	1.410
Cu-Al-(5,5)	end	0.036	2.72	2.63	1.390	1.327
	side	0.082	2.60	1.98	1.528	1.662
	embedded	0.094	2.78	1.78	1.406	1.503

walled system) contained 1692 atoms in its central region.

Good wettability reduces the metal-CNT electrical resistance by enhancing the contact area³⁴. Wetting properties can be theoretically described by combined analysis of the matrix internal surface energy²⁸ γ , the interface strength³² τ , and changes in CNT structure²⁶ described by the coefficient of CNT radius variation, CV¹⁶ (see ESI† for details). Formation of a continuous or quasi-continuous metallic layer adsorbed on the lateral surface of a nanotube is preferred when τ is high, whereas the separation tendency leading to the formation of a metal cluster is observed when γ is low. As expected^{21,28,41}, the presence of Ni significantly enhances CNT wetting (see Tab. 1). Further analysis of the dot, end, and side Ni contacts shows that increasing the number of Ni atoms (6, 21, and 64 atoms, respectively) improves metal-CNT binding but also severely disturbs the CNT structure, as indicated by the higher value of CV. The Ni embedded contact (85 Ni atoms) has higher γ but lower τ than the Ni side contact showing that the addition of Ni must be precisely controlled. Cr also improves CNT binding to the metal matrix, but not as much as Ni. Comparison of the embedded Ni and Cr contacts reveals that a high density of Cr does not alter the CNT structure as much as Ni, while a smaller density of Cr (end and side contacts) has an effect comparable to that of Ni. Interestingly, the greatest deformation of the CNT structure is observed in the Al-doped embedded system. The deformation even exceeds that observed in the Ni embedded case and is almost the same degree of distortion that can be induced by covalent functionalization¹⁶. Al atoms, which tend to create longer bonds with C atoms than do Cu atoms²¹, are trapped by surrounding Cu layers inside the composite and exhibit behaviour which is different from metal-CNT systems containing only one type of metal^{21,28}. The Cu-Al-CNT system is characterised by similar τ to the Cu-CNT system but smaller γ indicating that the introduction of Al between the Cu and CNT does not improve wetting.

To fully understand the character and origin of the interactions between the CNT and the metal matrix it is necessary to analyse the electronic properties of the composites and this is done by calculating the projected density of states (PDOS) and the energy resolved local device density of states (LDDOS). Fig. 4 shows the PDOS and LDDOS of all the Cu-M-CNT systems considered ac-

companied by side views of their structures. In contrast to previous studies of CNTs partially covered by Cu^{21,23,24} or filled with Cu⁴², the total DOS of the undoped Cu-CNT composite system does not resemble the intrinsic electronic structure of the pure CNT. It is mostly dominated by Cu states with only a minor contribution from C states as seen in Fig. 4 (a) and Fig.S5 (a) in the ESI†. There is very little sp²-sp³ rehybridization at the Cu-C interface and only weak coupling between Cu-d orbitals and C-p orbitals. These effects are most likely responsible for the inefficient conduction at the Fermi level described in earlier work³². We found that doping the Cu matrix with Ni or Cr introduces new electronic states at the Fermi level (see Fig. 4 (b) and (c)), which can contribute to electron injection and open new conducting channels in the composite. However, the number of conduction channels cannot be directly related to the conductance of the system. They determine only an upper limit. The new states have Ni-d and Cr-d character respectively and overlap with Cu-d and C-p states (see Fig.S5 (b) in the ESI†). In the Cu-Cr-CNT systems, the states are more broadened within the energy window around the Fermi level than in the Cu-Ni-CNT systems, which reflects differences in the strength of the bonding. The LDDOS of the Cu-Ni-CNT and Cu-Cr-CNT systems show an apparent electron accumulation between the alloying metal atom and the adjacent C atoms, which is not visible in the Cu-Al-CNT system (cf. Fig. 4 (b)-(d)). Al-p states are located below C-p states, which remain at the same level as in the undoped system; however, the density of Cu states at the Fermi level is slightly higher in the Cu-Al-CNT system than in the undoped system. This interesting effect is only seen for the Cu-Al-CNT composite with the end type contact and this contact is characterised by a smaller CV than the pure Cu-CNT system.

The electronic properties of a composite system are known to depend on the orientation of the CNT within the Cu matrix³². Consequently, other geometrical factors such as the size and type of the contact can also substantially influence the distribution of electronic states as well as their localization^{22,24,25}. Comparing the left and right hand regions of Fig. 4 (b) and (c), it is seen that electron injection, as represented by the LDDOS, is directly related to the number of alloying elements, since in this case there are 9 on the left end of the CNT and 11 on the right end. Furthermore, comparison of the DOS for the different types of contact

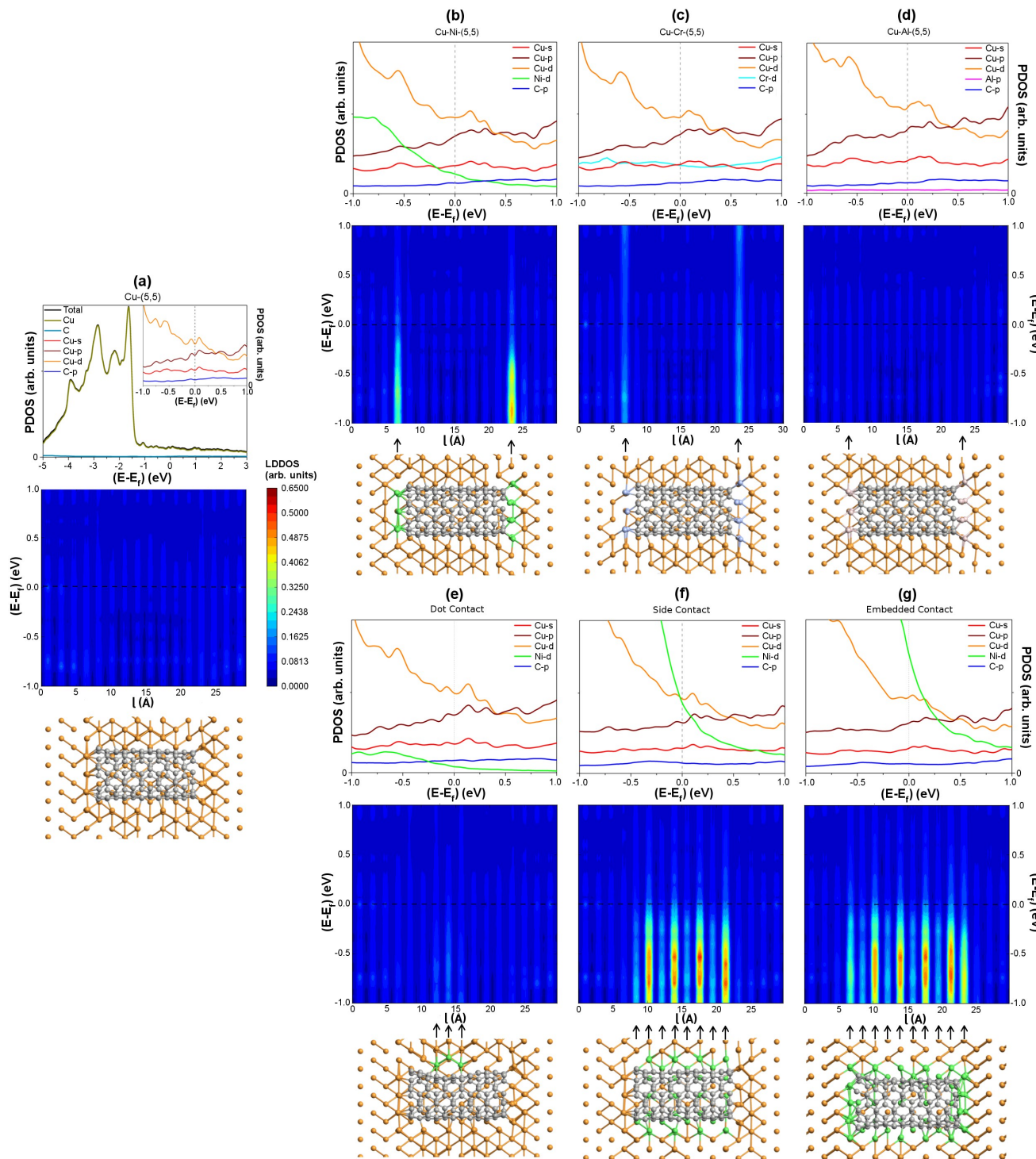


Fig. 4 Computed Electronic Properties of the Cu-M-CNT systems. Projected density of states (PDOS), energy resolved local device density of states (LDDOS) and side views of each system and contact type considered. (a) System without additional doping, (b)-(d) Ni-, Cr-, and Al-doped end type contact systems, (e)-(g) Ni-doped dot, side, and embedded contacts, respectively. Black arrows indicate the positions of the dopants.

(Fig. 4 (b), (e)-(g)) reveals that electron injection can also be controlled by the shape of the contact and its position with respect to the CNT geometry. For the Cu-Ni-CNT series shown in Fig. 4 (e)-(g), the increasing number of strongly interacting Ni atoms introduces more localised states as clearly visible in the

LDDOS maps. This, unfortunately, will hinder rather than facilitate electron transport since only delocalized states contribute to the transmission. Therefore, the number of Ni atoms with respect to the size of the CNT needs to be carefully adjusted so as to only create a connection between the CNT and the Cu matrix and not

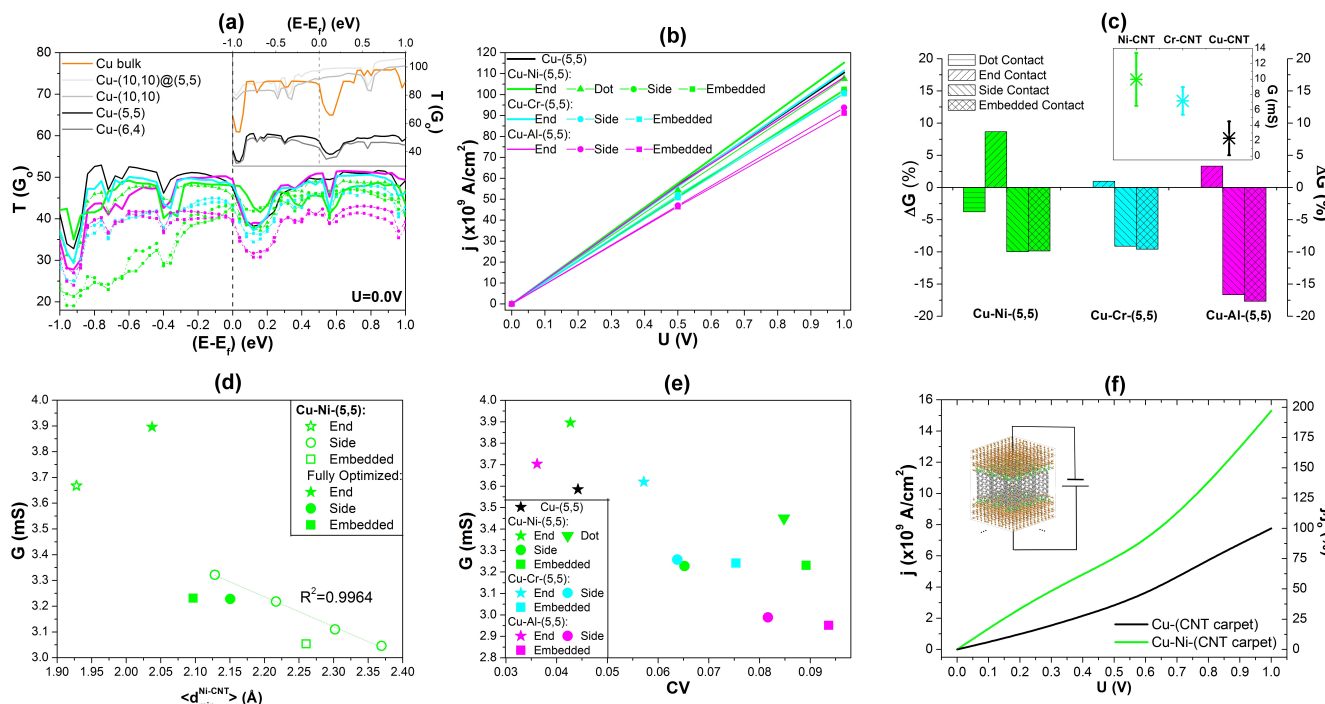


Fig. 5 Transport properties of the Cu-M-CNT composites and carpet systems. (a) The zero-bias transmission spectra for all metal alloy and contact types considered Inset: Comparison between the zero-bias transmission for bulk copper and pure Cu-CNT composites containing (5,5), (6,4), (10,10) and (10,10)(5,5) nanotubes. E_F is the Fermi energy. (b) The current density as a function of applied voltage for all Cu-M-CNT (5,5) composites and contact types considered (c) The relative change in conductance of Cu-M-CNT (5,5) composites with respect to the undoped system. Inset: The experimentally measured conductance of metal sputtered MWCNT tracks deposited on quartz plates after heat treatment. (d) The conductance as a function of the arithmetic mean of the minimal separation distance between C and Ni atoms. Fully optimized systems are indicated with closed symbols. Open symbols indicate systems that were not optimized after replacing the Cu atoms by Ni atoms. (e) The conductance as a function of the coefficient of variation of nanotube radius (CV) for all Cu-M-CNT (5,5) composites and contact types considered (f) The current density as a function of applied voltage for carpet systems with and without Ni alloying. Inset shows the computational model. The relative change in current density with respect to the undoped carpet system is depicted on the right axis. j_0 is the current density of an undoped system obtained when 1V is applied to the electrodes.

dissolve the nanotube or completely destroy its electronic properties. Besides the Ni end contact, the Ni dot contact seems to be the most promising, especially in the case of MWCNTs, since this system does not yield highly localised states (see LDDOS). We note that the dot contact type is experimentally achievable (see Fig. 3 (a)). Systems containing magnetic metals, such as Ni and Cr can present spin-selective transport properties.⁴³ Our spin-polarized calculations also show differences between both spin populations (see Fig.S5 (c)-(f) in the ESI†) although they are only significant at the Fermi level for the embedded contact.

The transport calculations focused on the Cu-M-CNT(5,5) system mainly for computational convenience although test calculations on CNTs of larger diameter, chiral character or with a double wall showed very similar trends in transmission behaviour (see Fig. 5 (a) inset and Fig.S6 (a) in the ESI†). The principal model size used (7x7x16) corresponds to a CNT density of about 3.0×10^{13} per cm^2 . The central part of the model is sandwiched between two semi-infinite copper electrode regions creating a system schematically shown in Fig. 1 (d). Zero-bias transmission spectra of the undoped systems presented in the inset in Fig. 5 (a) indicate that the conductance of composite is similar regardless of the semiconducting/metallic character of the nanotube due

to the metallization process induced by the presence of the metal matrix which is embedding the CNT^{21,25,32,43}. Comparison between composites containing single and double walls (Fig. 5 (a), inset) shows that the transmission through a double wall system is higher than a single wall system suggesting the participation of both walls in electrical transport. Fig.S6 (b) in the ESI† compares the transmission coefficients of two Cu-CNT composites with different CNT densities and shows that transmission and hence conductance, increases with decreasing CNT number density in agreement with previous computational work³². In particular the transmission coefficients can be increased by 272% by a 47% reduction in carbon concentration (wt%). The higher conductance of a system containing fewer nanotubes per unit area can be explained by structural changes in the Cu matrix near the incorporated CNTs induced by a lattice mismatch between these two materials. Fig.S6 (b) in the ESI† also shows that the difference in transmission at the Fermi level between bulk Cu and the composite decreases with decreasing CNT number density as expected. These results are in qualitative agreement with recent electrical measurements on vertically aligned Cu-CNT composite material^{4,44}.

Fig. 5 (a) shows that the transmission spectra over a particu-

lar energy window are similar for all composites considered indicating completely delocalized transport channels. Upon closer inspection, it is seen that end contacts are not only more promising than side contacts (Fig. 5 (a) and (b)) but also seem to be superior in conductance to fully embedded contacts (Fig 5 (c)). Since transport through a CNT occurs mainly along its symmetry axis, carrier injection will be most efficient at the CNT ends rather than over its lateral surface^{22,45}. Concentrating carriers around a CNT using a side contact increases back scattering in the system and reduces the overall conductance. Therefore, the embedded type of contact cannot reach the conductance level of the end contact. Interestingly, the electrical properties of the dot contact are better than the side and embedded contacts (see Fig. 5 (a)-(c)). Tuning the shape and size of the dot contact should allow the conductance of such a system to increase above that of the pure Cu-CNT composite with the end contact. Among the end contacts, Ni improves the conductance of the composite by 8.7%, while Cr and Al are also slightly better than the pure composite in the finite voltage range (see Fig. 5 (c) and Fig.S7 (a) in the ESI†). The latter result supports the idea of fabricating highly conductive Al-C^{12,46} material. It is worth noting that the calculated current densities shown in Fig. 5 (b) are three orders of magnitude higher (10^{11} A/cm²) than previously reported experimental values (10^8 A/cm²)⁸.

Enhanced current injection at a metal-CNT interface depends on a number of factors including favourable geometry and bonding, a high density of delocalized interface states at the Fermi level, and a low interfacial potential barrier which reduces contact resistance. Similar to graphene⁴⁷ and CNTs partially enclosed by metals²⁵, the separation distance between the CNT and the metal matrix in the composite become one of the dominant factors affecting the conductance of the system. Simple replacement of the first layer of Cu atoms around the CNT by M atoms (side contact) without any further geometry optimisation (empty circles in Fig. 5 (d)) shows that conductance is inversely proportional to the arithmetic mean of the minimal separation distance between the C and M atoms. This appears to be true for all types of contacts (cf. empty symbols in Fig. 5 (d)). The results show that the end contact has the smallest separation distance but after full geometry optimisation (full symbols) differences between the different contacts decreases. The LDDOS of the Ni side contact systems with different separation distances reveals striking differences in the electron distribution near the Fermi level (see Fig.S8 in the ESI†). A smaller separation distance facilitates charge transfer and maximises overlap of the wave functions between the metal matrix and the CNT. However, the reduced separation distance causes simultaneous structural change to other parts of the composite, the most serious being the disruption of the fragile sp² network of the CNT⁴⁸. As a consequence, the conductance of the composite system decreases with increasing CV (see Fig. 5 (e)). Our results are in agreement with experimental findings⁴⁹ which suggest that surface chemistry plays a crucial role in creating a good electrical contact between the metal and the CNT.

The last important factor is the contact resistance, the minimization of which requires a low and narrow potential barrier at the interface. A small electrostatic potential barrier implies more ef-

ficient carrier injection. According to recent work,²¹ Al-CNT and Ni-CNT contacts have higher contact resistance than Cu-CNT and Cr-CNT contacts. Interestingly though, our calculations indicate a different trend. This can be attributed to differences in models containing only a small number of M atoms connecting the Cu matrix with the CNT and those in which the CNTs are wrapped by several layers of one type of metal. For example, the barrier at the Cu-CNT composite is greater than the each of the barriers at the Cu-Ni-CNT, Cu-Cr-CNT or Cu-Al-CNT composites with either end or embedded contacts (see Tab. 1). This explains in particular why the Al end contact yields a higher current density than the Cu-CNT composite and comparable conductance. Unfortunately, Al and Cr become readily oxidized under ambient conditions. A result of this is the formation of a tunnelling barrier between the CNT and the metal matrix. Even if oxygen is removed from the composite the total amount of Al or Cr needs to be carefully controlled as an important factor influencing the morphology of the composite (see Fig.S1 in the ESI†) and accordingly its transport properties. The heights of the potential barriers clearly differ between types of contacts with the smallest being exhibited by the end contact. Importantly, the composite system with the lowest barrier is Cu-Ni-CNT (end contact).

In the ballistic regime the calculated transmission is directly related to the number of available conduction channels. However, in the NEGF approach, it is also possible to include higher order effects in the self-energies, consider nonlinear interactions and calculate the temperature dependence of the transmission function. Fig.S7 (b) in the ESI† shows how the conductance of each of the Cu-M-CNT composites with end contacts varies with temperature. There is a slight decrease with temperature in each case which could be important for heavy load applications⁸. Interestingly, the conductance of the Cr-doped system becomes lower than that of the pure Cu-CNT system for temperatures higher than 377° C. It is noted that that our calculated trend in the temperature dependence of the conductance correlates well with previous experimental observations⁸.

The most spectacular effect of Ni doping on Cu-M-CNT systems is found in carpet arrangements (Fig. 5 (f)). Carpets can be utilised in vertical vias within microelectronic interconnects (e.g. in batteries) but, as our experiments show, even nanoscale copper cannot penetrate the space between the CNTs when the carpets are dense. Therefore, our model presented in the inset of Fig. 5 (f), assumes a close packing of vertically aligned CNTs without any Cu atoms in between the nanotubes. The dimensions of the supercell along \hat{x} and \hat{y} are each reduced to approximately 10 Å. Consequently only the end type contact can be studied for this system. Due to the absence of Cu atoms between neighbouring CNTs, the potential barriers for holes and electrons at the interface between the metal matrix and the CNTs are almost 180% higher for Cu-(CNT carpet) system compared to Cu-CNT (embedded) (cf. Tab. 1 and Tab.S2 in the ESI†). This results in overall smaller current densities. However, introducing an appropriate amount of Ni at the end interface can resolve this problem. The right-hand potential barrier of the Cu-Ni-(CNT carpet) system (Tab.S2 in the ESI†) is even smaller than the corresponding barrier of the Cu-Ni-CNT end contact system because the CNT un-

dergoes smaller distortion (smaller CV) due to the absence of a surrounding Cu matrix. In contrast to the full composite (Fig. 5 (b)), the current-voltage characteristic of the carpet (Fig. 5 (f)) is non-linear due to inter-CNT coupling that lowers transmission at the Fermi level. The current density of the Ni-doped system increases gradually with applied voltage and becomes nearly a factor of two greater than the pure system when $U=1V$.

3 Conclusions

To conclude, we have demonstrated a simple and practical solution to the connection problem between CNTs and Cu. Our experiments and first principles calculations show that alloying the Cu with Ni or Cr can significantly improve wettability, adhesion and conductivity in Cu-CNT systems. Moreover, our calculations indicate that Ni, which is the most promising alloying element, can improve the conductance of Cu sputtered CNT carpets by a factor of 2 compared to the undoped system. In addition we predict that Al, which has the advantage of low density, can enhance the conductance of the composite even more than Cr in the low voltage regime. The results also identified the end and dot contact geometries as the most effective, and could easily be achieved experimentally. Furthermore, our theoretical model provides a clear interpretation of the physical origin of the superior electrical performance of Cu-M-CNT composites through the creation of a favourable interface geometry, an increase in the density of interface states contributing to the transmission, and a reduction in the contact resistance. We conclude that if designed and processed appropriately, Cu-M-CNT bimetal composites have great potential as novel conductors in a range of technologies including nanoscale electronics and macroscale applications in aerospace and transportation.

4 Methods

4.1 Fabrication and characterization of metal sputtered vertically aligned CNT carpets

The vertically aligned CNT (VACNT) carpets were synthesised using the floating catalyst CVD method and a feedstock based on a solution of ferrocene (Sigma Aldrich, 98%) in toluene (Fisher Scientific, general purpose grade). As-made carpets were sputtered with copper, chromium and nickel for 360 seconds at 80 mA (Emitech K575 Sputter Coater, Emitech Ltd., Ashford Kent, UK). Samples with dual coating were sputtered two times for 180 seconds using the same current. Heat treatment of the sputtered carpets was performed using a high vacuum furnace (Red Devil, Webb 134, USA) and target temperatures of 400° C, 600° C, 800° C and 1000° C. As-made and vacuum heated samples were dispersed in acetone using a Branson sonifier. SEM/EDX analysis was performed using a Nova NanoSEM 450 scanning electron microscope. Raman characterisations were made using a Renishaw Ramascope-1000 system. The Raman microscope system was equipped with a 633nm laser and a 1200-groove grating. This system can achieve a spectral resolution of 0.1 cm⁻¹, and spatial resolution of 1 micron.

4.2 Electrical Testing

The conductive CNT tracks on a nonconductive substrate were prepared by deposition of thin layers of CNT/acetone suspensions. The CNTs were synthesised using the floating catalyst CVD method and feedstock based on a solution of ferrocene (Sigma Aldrich, 98%) in toluene (Fisher Scientific, general purpose grade). The CNT tracks deposited on quartz plates were dried on a hot plate at 40°C for 12 hours and sputtered using an Emitech magnetron sputtering coater. The sputtered CNT tracks were vacuum heat treated at 800° C. The resistance of the CNT tracks was measured using a 2-probe method (Keithley 2000) after sputtering, vacuum heating and applying silver paint at the contact areas. The resistance of the electrical connections was very low in comparison to the sample resistance. Non-sputtered CNT tracks and Cr/Ni coatings sputtered directly on the nonconductive substrate were used as a reference.

4.3 Structural and electronic property calculations

The density functional theory (DFT)⁵⁰ calculations were performed within the Generalized Gradient Approximation (GGA) using the Perdew-Burke-Ernzerhof (PBE)⁵¹ parameterization with a double- ζ numerical orbital basis set localized on atoms and polarization functions (DZP) as implemented in the Atomistix ToolKit (ATK) and SIESTA numerical packages⁵². London dispersion interactions were included in the total bonding energy as proposed by Grimme⁵³. The kinetic energy cutoff for real-space integrals was set at 2040.85 eV and the Brillouin zone of the central part of the model was sampled using a 3x3x3 Monkhorst-Pack grid. The energy tolerance for the self-consistent calculations was set to 0.0027 eV. Further computational details are given in the ESI†.

4.4 Electron transport calculations

The coherent electron transport calculations were performed using the non-equilibrium Green's function (NEGF) technique within the Keldysh formalism (Ref. 52.b). All composite models were treated as two-probe systems with the central scattering region sandwiched between fully relaxed semi-infinite source (left) and drain (right) copper electrodes as illustrated in Fig. 1 (d). Both electrodes and their extensions (ee) in the central scattering part contain 7x7x2 (ca. 18.2 x 18.2 x 3.7 Å³) fully relaxed Cu atoms for the models containing the (5,5) and (6,4) CNTs. For the (10,10) and (10,10)@(5,5) CNTs the electrode regions were increased in size to 10x10x2 (ca. 25.9 x 25.9 x 3.7 Å³). The length of the electrodes together with the central region (ca. l_c=34 Å) was less than the electron mean free path in copper (ca. 400 Å) which defines the ballistic regime³². Due to the size of the system, the energy window for the calculation of the transport properties was chosen in the range of (-1,1) eV, within 51 points. The Brillouin zone of the two-probe system was sampled using a 1x1x100 Monkhorst-Pack grid. The calculations were performed at 300 K. Further computational details are provided in the ESI†.

5 Acknowledgement

This work was supported by the European Commission through the FP7-NMP programme (project UltraWire, grant No. 609057).

Computing resources were kindly provided by the Cambridge University High Performance Computing Cluster and the Interdisciplinary Centre for Mathematical and Computational Modeling at the University of Warsaw (Grant No. G47-5).

References

- 1 (a) G. E. Moore, *International Electron Devices Meeting*, 1975, 11–13; (b) M. M. Waldrop, *Nature*, 2016, **530**, 144–147.
- 2 B. K. Bose, *IEEE Industrial Electronics Magazine*, 2010, **4**, 6–17.
- 3 O. Hjortstam, P. Isberg, S. Soderholm and H. Dai, *Appl. Phys. A*, 2004, **78**, 1175–1179.
- 4 S. Sun, W. Mu, M. Edwards, D. Mencarelli, L. Pierantoni, Y. Fu, K. Jeppson and J. Liu, *Nanotechnology*, 2016, **27**, 335705.
- 5 S. I. Cha, K. T. Kim, S. N. Arshad, C. B. Moa and S. H. Hong, *Adv. Mater.*, 2005, **17**, 1377–1381.
- 6 W. M. Daoush, B. K. Lim, C. B. Mo, D. H. Nam and S. H. Hong, *Mater. Sci. Eng. A*, 2009, **513–514**, 247–253.
- 7 S. M. Uddin, T. Mahmud, C. Wolf, C. Glanz, I. Kolaric, C. Volkmer, H. Höller, U. Wienecke, S. Roth and H.-J. Fecht, *Comput. Scienc. Tech.*, 2010, **70**, 2253–2257.
- 8 C. Subramaniam, T. Yamada, K. Kobashi, A. Sekiguchi, D. N. Futaba, M. Yumura and K. Hata, *Nature Comm.*, 2013, **4**, 2202.
- 9 K. T. Kim, J. Eckert, S. B. Menzel, T. Gemming and S. H. Hong, *App. Phys. Lett.*, 2008, **92**, 121901.
- 10 G. Chai, Y. Sun, J. J. Sun and Q. Chen, *J. Micromech. Microeng.*, 2008, **18**, 035013.
- 11 C. Subramaniam, Y. Yasuda, S. Takeya, S. Ata, A. Nishizawa, D. Futaba, T. Yamada and K. Hata, *Nanoscale*, 2014, **6**, 2669–2674.
- 12 S. R. Bakshi, D. Lahiri and A. Agarwal, *Inter. Mater. Rev.*, 2010, **55**, 41–64.
- 13 E. Bekyarova, E. T. Thostenson, A. Yu, M. E. Itkisa, D. Fakhrutdinov, T.-W. Chou and R. C. Haddon, *J. Phys. Chem. C*, 2007, **111**, 17865–17871.
- 14 K. Z. Milowska, *PhD thesis*, University of Warsaw, Warsaw, 2013.
- 15 K. Z. Milowska and J. A. Majewski, *J. Chem. Phys.*, 2013, **138**, 194704.
- 16 K. Z. Milowska, *J. Phys. Chem. C*, 2015, **119**, 26734–26746.
- 17 J. Zhao, A. Buldum, J. Han and J. P. Lu, *Nanotech.*, 2002, **13**, 195–200.
- 18 D. Janas, K. Z. Milowska, P. D. Bristowe and K. K. K. Koziol, *Nanoscale*, 2017, **9**, 3212–3221.
- 19 K. Ji, H. Zhao, J. Zhang, J. Chen and Z. Dai, *App. Surf. Science*, 2014, **311**, 351–356.
- 20 C. Kim, B. Lim, B. Kim, U. Shim, S. Oh, B. Sung, J. Choi, J. Ki and S. Baik, *Synt. Met.*, 2009, **159**, 424–429.
- 21 A. Fediai, D. A. Ryndyk, G. Seifert, S. M. M. Claus, M. Schröter and G. Cunibertia, *Nanoscale*, 2016, **8**, 10240–10251.
- 22 F. Gao, J. Qu and M. Yao, *Appl. Phys. Lett.*, 2010, **96**, 102108.
- 23 F. Gao, J. Qu and M. Yao, *Physica E*, 2011, **44**, 146–151.
- 24 A. Zienert, J. Schuster and T. Gessner, *Nanotechnology*, 2014, **25**, 425203.
- 25 M. B. Nardelli, J.-L. Fattebert and J. Bernhole, *Phys. Rev. B*, 2001, **64**, 245423.
- 26 A. Maiti and A. Ricca, *Chem. Phys. Lett.*, 2004, **395**, 7–11.
- 27 W. Zhu and E. Kaxiras, *Nano Lett.*, 2006, **6**, 1415–1419.
- 28 Y. He, J. Zhang, Y. Wang and Z. Yu, *Appl. Phys. Lett.*, 2010, **96**, 063108.
- 29 Y. Feng and S. L. Burkett, *Comput. Mater. Sci.*, 2014, **97**, 1–5.
- 30 I. Awad and L. Ladani, *J. Nanotechnol. Eng. Med.*, 2014, **4**, 041001.
- 31 I. Awad and L. Ladani, *J. Nanotechnol. Eng. Med.*, 2014, **5**, 031007.
- 32 M. Ghorbani-Asl, P. D. Bristowe and K. Koziol, *Phys. Chem. Chem. Phys.*, 2015, **17**, 18273–18277.
- 33 M. Burda, *PhD thesis*, Silesian University of Technology, Gliwice, 2013.
- 34 M. Burda, A. Łekawa-Raus, A. Gruszczyk and K. K. K. Koziol, *ACS Nano*, 2015, **9**, 8099–8107.
- 35 (a) P. R. Couchman and W. A. Jesser, *Nature*, 1977, **269**, 481–483; (b) F. Delogu, *Phys. Rev. B*, 2005, **72**, 205418; (c) Y. Shibusawa and T. Suzuki, *Chem. Phys. Lett.*, 2010, **498**, 323–327.
- 36 (a) J. R. Anderson, *MSc thesis*, Massachusetts Institute of Technology, 1946; (b) M. Nicholson, *Trans. Metall. Soc. AIME*, 1962, **224**, 533–535; (c) H. Sueyoshi and H. Fukudome, *Mat. Trans.*, 2008, **49**, 2063–2067.
- 37 (a) H. O. Pierson, *Handbook of refractory carbides and nitrides*, Noyes Publications, 1996; (b) T. Y. Kosolapova, *Carbides: Properties, Production, and Applications*, Springer, 2012.
- 38 L. Ramqvist, *J. Powd. Metall.*, 1965, **1**, 2–21.
- 39 N. Eustathopoulos, M. Nicholas and B. Drevet, *Wettability at High Temperatures*, Pergamon, 1999, vol. 3.
- 40 J. Günter, *Copper: Its Trade, Manufacture, Use, and Environmental Status*, Pergamon, 1998.
- 41 Y. Zhang, N. W. Franklin, R. J. Chen and H. Dai, *Chem. Phys. Lett.*, 2000, **331**, 35–41.
- 42 J. Jiang, C. Yang and Q. Chen, *J. Min. Met. Mat. Soc.*, 2016, **68**, 311–317.
- 43 (a) A. N. Andriotis and M. Menon, *Phys. Rev. B*, 2007, **76**, 045412; (b) Y. Yang, Y. Xiao, W. Ren, X. H. Yan and F. Pan, *Phys. Rev. B*, 2011, **84**, 195447.
- 44 P.-M. Hannula, A. Peltonen, J. Aromaa, D. Janas, M. Lundström, B. P. Wilson, K. Koziol and O. Forsén, *Carbon*, 2016, **107**, 281–287.
- 45 F. Gao, J. Qu and M. Yao, *Appl. Phys. Lett.*, 2011, **98**, 172103.
- 46 D. G. Kvashnin, M. Ghorbani-Asl, D. V. Shtansky, D. Golberg, A. V. Krasheninnikov and P. B. Sorokin, *Nanoscale*, 2016, **8**, 20080–20089.
- 47 Q. Gao and J. Guo, *APL Materials*, 2014, **2**, 956105.
- 48 F. Gao, J. Qu and M. Yao, *Appl. Phys. Lett.*, 2010, **97**, 242112.
- 49 S. C. Lim, J. H. Jang, D. J. Bae, G. H. Han, S. Lee, I.-S. Yeo and Y. H. Lee, *App. Phys. Lett.*, 2009, **95**, 264103.
- 50 (a) P. Hohenberg and W. Kohn, *Phys. Rev.*, 1964, **136**, B864–

- B871; (b) W. Kohn and L. Sham, *Phys. Rev.*, 1965, **140**, A1133–A1138.
- 51 J. P. Perdew, K. Burke and M. Ernzerhof, *Phys. Rev. Lett.*, 1996, **77**, 3865–3868.
- 52 (a) Atomistix ToolKit version 2015, QuantumWise A/S, (www.quantumwise.com); (b) M. Brandbyge, J.-L. Mozos, P. Ordejon, J. Taylor and K. Stokbro, *Phys. Rev. B*, 2002, **65**, 165401; (c) J. M. Soler, E. Artacho, J. D. Gale, A. Garcia, J. Junquera, P. Ordejon and D. Sanchez-Portal, *J. Phys.: Condens. Matter*, 2002, **14**, 2745.
- 53 S. Grimme, *J. Comput. Chem.*, 2006, **27**, 1787–1799.